

Timing and Spectral Studies of the X-ray Pulsar 2S 1417–624 During the Outburst in 2021

Manoj Mandal

Midnapore City College, Kuturia, Bhadutala, West Bengal, India

and

Sabyasachi Pal

Midnapore City College, Kuturia, Bhadutala, West Bengal, India

ABSTRACT

We have studied the evolution of different timing and spectral properties of the X-ray pulsar 2S 1417–624 during the recent outburst in January 2021 based on the Neutron Star Interior Composition Explorer (NICER) observations. The spin period during the outburst is $P \sim 17.3622$ s based on the NICER data and the period decreases slowly with time. The evolution of the spin period and pulsed flux is studied with Fermi/GBM during the outburst and the spin-up rate was found to be varied between $\simeq (0.8\text{--}1.8) \times 10^{-11}$ Hz s $^{-1}$. The pulse profile shows strong energy dependence and variability. The pulse profile shows multiple peaks and dips which evolve significantly with energy. The pulsed fraction shows a positive correlation with energy. The evolution of the spectral state is also studied. The NICER energy spectrum is well described with a composite model of – power-law and a blackbody emission along with a photo-electric absorption component. An iron emission line is detected near 6.4 keV in the NICER spectrum with an equivalent width of about 0.05 keV. During the recent outburst, the flux was relatively low compared to the 2018 outburst and the mass accretion rate was also low. The mass accretion rate is estimated to be $\simeq 1.3 \times 10^{17}$ g s $^{-1}$ near the peak of the outburst. We have found a positive correlation between the pulse frequency derivatives and luminosity. The GL model was applied to estimate the magnetic field in low mass accretion rate and different spin-up rates, which is compared to the earlier estimated magnetic field at a relatively high mass accretion rate. The magnetic field is estimated to be $\simeq 10^{14}$ G from the torque-luminosity model, which is comparatively higher than most of the other Be/XBPs.

Subject headings: accretion, accretion disks - star: pulsar, individual: 2S 1417–624.

1. Introduction

The X-ray transient pulsar 2S 1417–624 was discovered using Small Astronomy Satellite (SAS-3) in 1978 (Apparao et al. 1980). Several outbursts from the source were observed by BATSE and Rossi X-ray Timing Explorer (RXTE) (Finger et al. 1996a; Gupta et al. 2018). Earlier, X-ray pulsation at ~ 17.5 s were detected in the source light curve with an orbital period of ~ 42 days (Finger et al. 1996a). The orbital parameters of the binary system were improved by Raichur & Paul (2010) using RXTE during the giant outburst in 1999.

The accretion-powered X-ray pulsar 2S 1417–624 went through a giant outburst in 2009 and different timing and spectral properties were studied during the outburst using RXTE (Gupta et al. 2018). During this outburst, the pulse profile showed energy and luminosity dependence, and the pulse profile evolved from a double-peak feature in lower luminosity to a triple-peak feature at higher luminosity and get back to a double-peak feature during the decay phase of the outburst. The variation of pulse fraction was studied with flux, which showed an anti-correlation with source flux during the outburst.

During the 2018 giant outburst, the source was studied in multi-wavelength using Swift, NuSTAR (Gupta et al. 2019), NICER, and Insight-HXMT (Ji et al. 2020). During the NuSTAR observation, the strong energy dependence of the pulse profile was observed and the four-peaked pulse profile at lower energies evolved into a double peak feature at higher energies. The pulse fraction showed an anti-correlation with luminosity, which was similar to the previous giant outburst in 2009 (Gupta et al. 2019).

The variability in the pulse profile was also observed from the NICER observations and the geometry of the pulse profile evolved significantly with luminosity and energy (Ji et al. 2020). The magnetic field was estimated by considering the spin-up due to the accretion torque to be $\sim 7 \times 10^{12}$ G.

Recently, the source went through an outburst that was strongest after the giant outburst of 2018. The outburst was detected by Fermi/GBM, Burst Alert Telescope (BAT) onboard Swift and Gas Slit Camera (GSC) onboard MAXI on January 2021 (Hazra et al. 2021). The X-ray flux started to increase from the early last week of January 2021 and the duration of the outburst was nearly two months. In this paper, we have studied the timing and spectral properties of the pulsar 2S 1417–624 during the recent outburst in 2021 using NICER observation and compare different timing and spectral properties with the giant outburst of 2018. We have discussed the data reduction and analysis method in Section 2. We have summarized the result of the current study in Section 3. The discussion and conclusion are summarized in the Section 4 and 5 respectively.

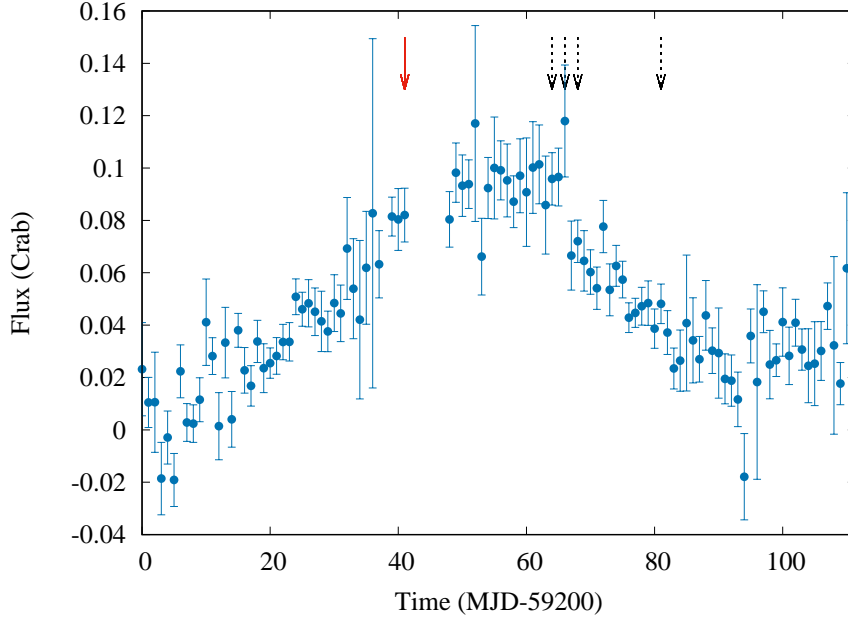


Fig. 1.— Outburst from X-ray pulsar 2S 1417–624 was detected by Swift/BAT (15–50 keV) during January–February 2021. The red solid arrow shows the time of NICER observation and the black dotted-arrows show the time of Swift observations.

2. Observation and data analysis

We have detected an outburst from the X-ray pulsar 2S 1417–624 and followed the evolution of the outburst using different instruments. We use data from all-sky X-ray monitors like Swift/BAT (15–50 keV), MAXI/GSC (2–20 keV), Fermi/GBM (12–50 keV). We analyzed the NICER data during the rising phase of the 2021 outburst and Swift/XRT data, close to the peak of the outburst. We used the `HEASOFT` v6.27.2 for the data reduction and analysis.

BAT onboard the Swift observatory ([Gehrels et al. 2004](#)) is sensitive in hard X-ray (15–

Table 1: Log of NICER observations

Instrument	Start time (MJD)	Date (yyyy-mm-dd)	Exposure (ks)	Observation id
NICER	59241	2021-01-27	7.165	3200130112
	58308.25	2018-07-09	1.745	1200130165
	58282.67	2018-06-13	1.778	1200130149
	58296.28	2018-06-27	1.423	1200130155

50 keV) (Krimm et al. 2013). We have used the results of the BAT transient monitor during the outburst, which is provided by the BAT team. BAT flux reached a maximum of ~ 100 mCrab during the first week of February and continued for ~ 2 months.

The Neutron Star Interior Composition Explorer (NICER) was launched in 2017 and working as an external payload on the International Space Station. NICER consists of one instrument, the X-ray Timing Instrument (XTI) and operating in soft X-ray region (0.2–12 keV) (Gendreau et al. 2016). A follow-up observation was conducted by NICER on January 27, 2021, in the rising phase of the flare, close to the peak of the outburst. The detail of the NICER observation is tabulated in Table 1. The processing of raw data has been done using the NICERDAS in HEASOFT v6.27.2 with the latest caldb version. We have created clean event files by applying the standard calibration and filtering tool `nicer12` to the unfiltered data. We have extracted light curves and spectra using `XSELECT` from the barycenter corrected reprocessed clean event file. For the timing analysis, we selected good time intervals according to the following conditions: ISS not in the South Atlantic Anomaly (SAA) region, source elevation $> 20^\circ$ above the Earth limb, source direction at least 30° from the bright Earth. For timing analysis, we have applied barycentric corrections to those events using the task `barycorr`. The ancillary response file and response matrix file of version 20200722 were considered in our spectral analysis. The background corresponding to each epoch of the observation was simulated by using the `nibackgen3C50`¹ tool (Remillard et al., in prep.). Ancillary response file and response matrix file of version 20200722 are considered in our spectral analysis. We have used the latest response file for the spectral analysis.

The Fermi Gamma-ray Space Telescope operates within a wide energy range between 8 keV–40 MeV. The Large Area Telescope (LAT) and Gamma-ray Burst Monitor (GBM) are two main instruments onboard the Fermi Gamma-ray Space Telescope (Meegan et al. 2009). The GBM is made up of 14 detectors: 12 detectors of Sodium Iodide (NaI) and 2 detectors of Bismuth Germanate (BGO). In the current study, we have used the spin frequency, frequency derivative, and 12–50 keV pulsed flux measurements with the Fermi/GBM (Finger et al. 2009). The outburst from 2S 1417–624 was also detected with Fermi/GBM from January 2021 and continued for nearly two months with a maximum pulsed flux of ~ 0.27 keV cm⁻² s⁻¹ on MJD 59260 as provided by Fermi/GBM (Meegan et al. 2009). The spin-frequency and frequency derivative are also used, which is estimated by the Fermi/GBM. There were a total of 23 spin frequency (ν) measurements conducted during our study and we have used 18 measurements, which were at around 3-d equal intervals and we have not included the first and last few measurements. We used a linear function to fit each three consecutive

¹https://heasarc.gsfc.nasa.gov/docs/nicer/tools/nicer_bkg_est_tools.html

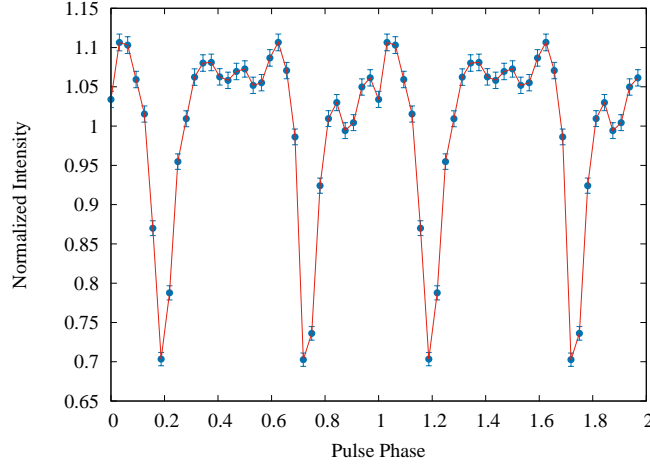


Fig. 2.— The pulse profile of 2S 1417–624 using NICER/XTI (0.3–12 keV) with best period 17.3622 s.

frequency measurements with time. The spin-up rate was calculated from the slope of the linear function during a 9-d interval, as each pulse frequency measurement was collected every 3-d interval, using the χ^2 minimization technique. We repeated this process for the next three frequency measurements and so on (viz. Kabiraj & Paul (2020)). Therefore, we had 6 spin-up rates from 18 spin frequencies. We have used the average value of total flux for three consecutive points over the same intervals, which are used to determine $\dot{\nu}$. Finally, the luminosity is estimated from the X-ray flux for a distance of ~ 10 kpc. X-ray luminosity of the source is calculated from the count rate history provided by swift/BAT team (Krimm et al. 2013) by multiplying a flux conversion factor of 1.13×10^{-7} erg cts $^{-1}$ (Ji et al. 2020).

We have made use of MAXI/GSC (2–20 keV) light curves data (Matsuoka et al. 2009) to follow up the outburst and to study the evolution of spectral states. MAXI in-orbit operation was started in 2009 and nearly 300 pre-registered sources have been monitored at a regular interval in different energy bands 2–4 keV, 4–10 keV, and 10–20 keV bands. The data provided by MAXI/GSC are averaged for every day. We have studied the evolution of the hardness of the X-ray pulsar using data from different energy bands.

2.1. Timing analysis

The light curve was produced using the science event data in different energy ranges with bin size 0.1 s for the NICER data. We used the `efsearch` task in FTTOOLS to check for

the periodicity in the time series of the barycenter and background corrected data set. We used the folding method of the light curve over a trial period to get the best period by χ^2 maximizing process (Leahy 1987) over 32 phase bins in each period. After getting the best spin period, pulse profiles were generated using the `efold` task in `FTOOLS` by folding light curves with the best spin period. The evolution of the pulse period and pulsed flux during the outburst was studied using time-series data from the Fermi/GBM.

2.2. Spectral analysis

X-ray spectrum has been produced using the NICER (0.7–12 keV) data. We excluded the spectrum above 12 keV and below 0.7 keV due to the poor source count rate statistics in this range. Swift observed the source during the declining phase of the outburst. The source count statistics for the Swift/XRT observations were very poor and exposure was also very low.

The NICER spectrum was fitted using `XSPEC` v12.11.0 and model parameters were varied independently. We tried different simple single-component models like power-law, `bbbody`, `compTT` as well as combinations of models like power-law+`bbbody`, `diskbb`+`bknpower`, `diskbb`+`compTT`, `compTT`+`bknpower` to fit the source spectrum. The spectrum was well fitted with a blackbody emission with a power-law component and an iron emission line at 6.4 keV also models using a Gaussian. The blackbody has been introduced along with a simple power-law to model the soft excess component (Hickox et al. 2004). To find the effect of absorption by hydrogen, all model components were multiplied by a photo-electric absorption model.

3. Results

The X-ray pulsar 2S 1417–624 went through an outburst during January–February 2021, detected by Fermi/GBM, Swift/BAT² and MAXI/GSC which reached a maximum flux during the second week of February 2021. Fig. 1 shows the variation of hard X-ray flux during the outburst using Swift/BAT (15–50 keV). The total duration of the outburst was around 2 months which started in early January 2021 and continued till February 2021. We have summarized the result of timing and spectral analysis of 2S 1417–624 during the recent outburst in 2021.

²<https://swift.gsfc.nasa.gov/results/transients/>

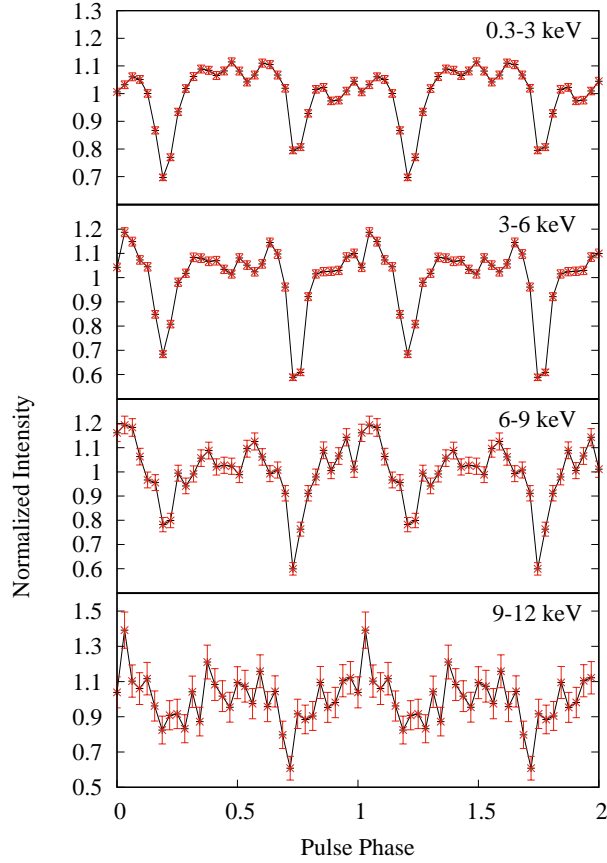


Fig. 3.— Energy dependent pulse profile of the X-ray pulsar 2S 1417–624 using NICER/XTI observation. Pulse profiles were normalized to count rate such that the average count rate is 1 and total count rate is 32.

3.1. Variation of pulse profile and pulse fraction

We have studied the variation of different timing properties of the X-ray pulsar 2S 1417–624 during the outburst using Swift and NICER observations. The spin period of the pulsar during the outburst is found to be $P = 17.3622 \pm 0.0001$ s using NICER data, which is comparable with the pulse period recorded with Fermi/GBM³ during the outburst. Fermi/GBM found that the period is decreased slowly with the time of the flare. Fig. 2 shows the pulse profile using NICER/XTI data in the energy range 0.3–12 keV, which consists of multiple broad peaks and narrow dips. We did not find strong and significant pulsation from XRT observations probably due to poor count statistics and low exposure.

³<https://gamma-ray.nsstc.nasa.gov/gbm/science/pulsars>

We also looked for the energy dependence of the pulse profile as well as the temporal variation of the pulse profile during the outburst. Fig. 3 represents the energy-dependent pulse profile for four different energy ranges. The variation of the pulse profile over four energy bands: 0.3–3 keV, 3–6 keV, 6–9 keV and 9–12 keV is shown in Fig. 3. The pulse profile shows a strong energy dependence. The pulse profile shows two broad peaks and dips, which varied with energy. The pulse profile of the first row (0.3–3 keV) of Fig. 3 shows two clear dips and two broad peaks.

For estimating the rms PF, we used a simple formula,

$$PF = \frac{1}{\sqrt{N}} \left[\sum_{i=1}^N p_i - \bar{p} \right]^{\frac{1}{2}} \quad (1)$$

where N is the total number of phase bins, p_i is the count rate in the i th phase bin of the pulse profile, and \bar{p} is the average count rate. Fig. 4 shows the variation of rms PF for different energy ranges for which the energy-resolved pulse profile is studied and horizontal bars represent the energy ranges for which the PF is calculated and the vertical bars indicate the corresponding error in measurements. The rms PF shows a positive correlation with energy.

We have studied the evolution of the spectral state of the source during the outburst. Fig. 6 shows the variation of flux using Swift/BAT and MAXI/GSC. The bottom panel of Fig. 6, shows that the spectral state changes from soft to hard at the time of the rising phase of the outburst, during the time MJD 59210–59250 and hardness ratio reaches a maximum near the peak of the outburst. The hardness ratio has started to decrease from MJD 59255 and the state changes from harder to softer.

Fig. 5 shows the evolution of the spin frequency and pulsed flux (12–50 keV) during the outburst using Fermi/GBM, which implies that the pulse period of the X-ray pulsar has decreased slowly with time. We estimated the spin frequency derivative (as described in section 2), which varied between $\sim 0.8\text{--}1.8 \times 10^{-11}$ Hz s $^{-1}$ during the outburst.

Fig. 7 shows the variation of spin-up rate with luminosity. A power-law is used to fit the $\dot{\nu}$ and luminosity. This shows a positive correlation between the spin-up rate and the luminosity.

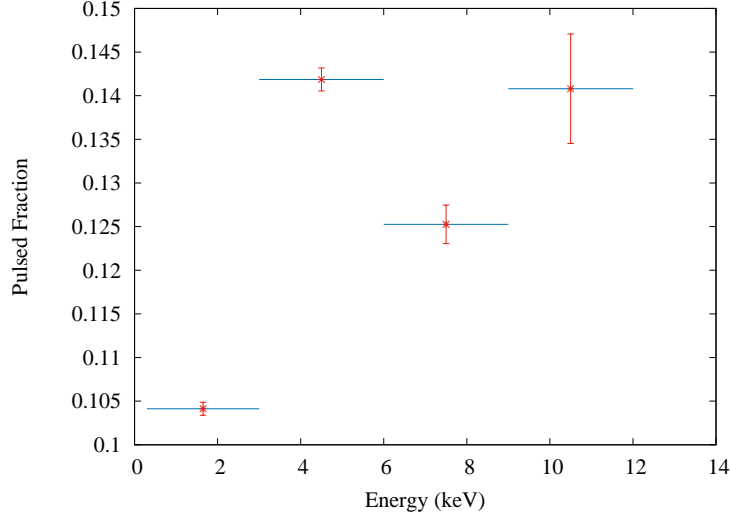


Fig. 4.— Variation of pulse fraction with energy using NICER/XTI. The horizontal lines represent the corresponding energy ranges for which PF is estimated.

3.2. Energy spectrum

We have studied the energy spectrum using NICER/XTI data and compare the variation of spectral parameters near the same flux level of the earlier outburst. Earlier, the spectrum of the source was modeled using absorbed power-law with a high energy cut-off and an iron emission line near 6.4 keV (Gupta et al. 2019). We have applied an absorbed power-law continuum model and an additional blackbody emission is introduced which improves the fit statistics. This model is good enough to describe the spectral continuum at lower flux limits, which becomes more complex at higher flux levels as observed during the giant outburst of 2018 (Gupta et al. 2019). The additional emission near 6.4 keV is modeled using a Gaussian component, which provides a reduced χ^2 value of ~ 1.0 . The radius of the BB emission

Table 2: Spectral fitting parameters for best fitted models for NICER/XTI (0.7–10 keV) observations:

Obs. ID	Date	Count rate	N_H	Photon index (Γ)	kT_{bb}	Line energy	Equivalent width	χ^2 (d.o.f)	Flux (10^{-10})
	(MJD)	(Count s $^{-1}$)	(10^{22} , cm $^{-2}$)		(keV)	(keV)	(keV)		(erg cm $^{-2}$ s $^{-1}$)
3200130112	59241	39.85 \pm 0.08	1.24 \pm 0.05	1.34 \pm 0.17	2.85 \pm 0.06	6.39 \pm 0.03	0.05 \pm 0.03	1.06 (921)	5.318 \pm 0.005
1200130165	58308.25	40.23 \pm 0.15	1.30 \pm 0.10	1.70 \pm 0.30	2.60 \pm 0.10	6.43 \pm 0.08	0.09 \pm 0.04	1.14 (921)	5.775 \pm 0.006
1200130149	58282.67	57.84 \pm 0.24	1.11 \pm 0.08	0.90 \pm 0.30	3.16 \pm 0.50	6.44 \pm 0.14	0.38 \pm 0.13	1.00 (921)	8.014 \pm 0.004
1200130155	58296.28	52.06 \pm 0.18	1.32 \pm 0.08	1.50 \pm 0.25	2.93 \pm 0.13	6.46 \pm 0.06	0.13 \pm 0.07	1.05 (921)	7.582 \pm 0.004

Model : phabs*(powerlaw+bbbody+gaussian), N_H : hydrogen column density, Γ : power-law photon index, kT_{bb} : blackbody temperature

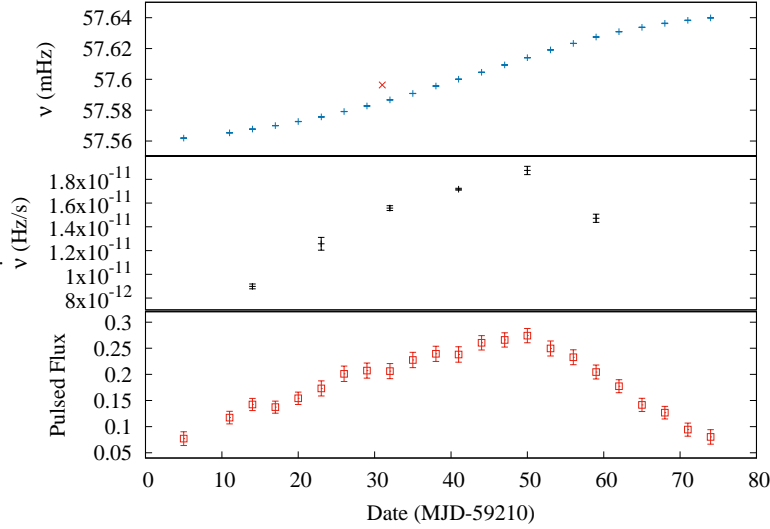


Fig. 5.— The first panel shows the variation of pulse frequency (ν) during the flare using Fermi/GBM. The pulse frequency estimated using NICER is shown in a red cross. The second panel represents the variation of frequency derivatives ($\dot{\nu}$), which is estimated from Fermi GBM spin period evolution history. The third panel shows the evolution of pulsed flux (12–50 keV) in the unit $\text{keV cm}^{-2} \text{s}^{-1}$ using Fermi/GBM. The vertical bars represent the error of corresponding measurements.

region is estimated using the normalization of the BB model. The energy spectrum with the best-fitted models is shown in Fig. 8 where the bottom panels of the Fig. 8 show the residuals. The energy spectrum of the X-ray pulsar can be well fitted with a power-law (`powerlaw` in `XSPEC`) and blackbody emission component (`bbbody` in `XSPEC`) along with a photoelectric absorption (`phabs` in `XSPEC`). The NICER spectrum in the energy range 0.7–12 keV is well described with blackbody emission with temperature (kT_{bb}) ~ 2.8 keV with hydrogen column density $\sim 1.2 \times 10^{22} \text{ cm}^{-2}$. The NICER X-ray flux in the 0.7–12 keV energy range is $\sim 5.0 \times 10^{-10} \text{ ergs cm}^{-2} \text{s}^{-1}$. Table 2 shows the different spectral parameters for the best-fitted values. We have also looked for the variation of spectral parameters with X-ray flux. The source has experienced a significant change in its spectral shape. The photon index decreased as the flux increased and showed a negative correlation below the flux level of $8 \times 10^{-10} \text{ erg cm}^{-2} \text{s}^{-1}$, which implies at the brighter phase of the source the X-ray emission was harder. Near the peak of the outburst, the photon index was ~ 1.3 . We have used few earlier NICER data near the same flux level for the sake of comparison. The photon index showed a consistent value with the earlier observation at the same flux level. Hydrogen column density and the blackbody temperature also did not show any significant variation in the same flux level.

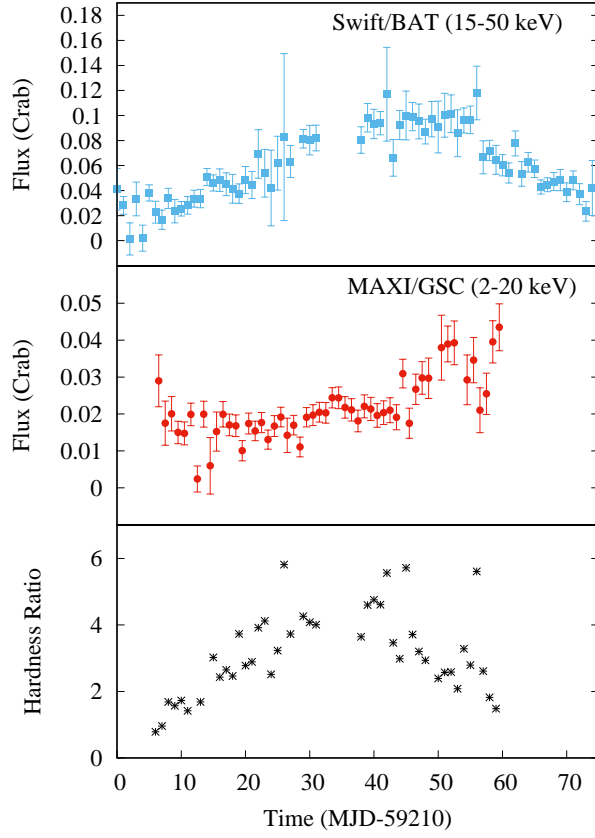


Fig. 6.— The first row shows the evolution of flux using Swift/BAT and the second row shows the evolution of flux using MAXI/GSC during the outburst of 2021. The third row shows the variation of hardness ratio (BAT/MAXI) during two outbursts.

4. Discussion

We present the results of timing and spectral analysis of 2S 1417–624 using the NICER and Swift data during the recent outburst in 2021. The timing analysis reveals that the pulse profile shows multiple peaks and dips with an energy-dependent nature, which is comparable with the previous results during the giant outbursts in 2009 (Gupta et al. 2018) and 2018 (Ji et al. 2020; Gupta et al. 2019). The energy dependence of the pulse profile is studied to investigate the evolution of the individual dips, peaks of the pulsar with different energies. The geometry of the pulse profile evolves significantly with energy, which is consistent with the previous result (Ji et al. 2020). The pulse fraction shows a trend to increase with energy, which is consistent with the 2018 giant outburst (Gupta et al. 2019). The spin-up rate is found to vary from 0.8×10^{-11} Hz s $^{-1}$ to 1.8×10^{-11} Hz s $^{-1}$ during the outburst, which is comparable to the previous outbursts of 2S 1417–624 (Finger et al. 1996a; Ji et al. 2020).

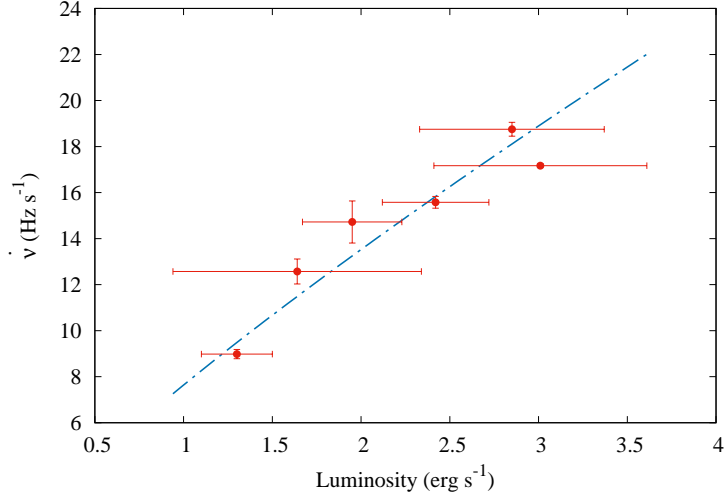


Fig. 7.— Variation of spin change rate in unit of $10^{-12} \text{ Hz s}^{-1}$ with luminosity in unit of $10^{37} \text{ erg s}^{-1}$. The solid line represents the best power-law fit of data points that give a power-law index of 0.82 ± 0.11 .

The mass accretion rate is estimated using the luminosity near the peak (during NICER observation) of the outburst as, $L = \eta \dot{M} c^2$ and $\dot{M} = 1.3 \times 10^{17} \text{ g s}^{-1}$, which is estimated using $\eta = 0.2$.

Earlier the X-ray pulsar 2S 1417–624 showed strong luminosity and energy dependence during the 2018 giant outburst. During the present outburst, multiple peaks and dips are observed in the pulse profile for different transient Be/XBPs and pulse profiles evolved significantly with energy. Several pulsars show energy and luminosity dependence of the pulse profiles like A 0535+262 (Mandal & Pal 2020), EXO 2030+375 (Epili et al. 2017; Naik et al. 2013), GX 304–1 (Jaisawal et al. 2016).

The luminosity during the NICER observation of 2021 outburst was below $\sim 2.5 \times 10^{37} \text{ erg s}^{-1}$ and at this phase of the outburst, the pulse profile showed two broad peaks, which is consistent with the previous result (Ji et al. 2020) and the emission geometry is expected to be driven by “pencil beam” pattern during this sub-critical accretion regime. During the recent outburst, multiple dips-like features were observed from 2S 1417–624, which are believed to be originated due to absorption or obscuration of X-ray photon by a narrow stream of matter. The typical value of the critical luminosity of accretion powered X-ray pulsars are estimated to be in the order of $10^{37} \text{ erg s}^{-1}$ (Becker et al. 2012; Reig & Nespoli 2013). This critical value of luminosity is important to understand the transition between sub-critical and super-critical accretion regimes. In sub-critical phases the emission geometry

is comparatively simple, the accretion flow is supposed to halt by Coulomb interaction close to the neutron star surface. The single or double-peaked pulse profile is produced and emission geometry can be driven by a pencil beam-like pattern. Earlier, in the 2018 outburst, the luminosity was higher and near the critical luminosity the beam geometry changed and multiple peaks were observed in pulse profile (Gupta et al. 2018). The emission geometry was changed from a pencil beam to a mixture of pencil and fan beams.

We look at the hardness ratio (HR) using the ratio of the count rates with time from Swift/BAT (15–50 keV) and MAXI/GSC (2–20 keV) to study the evolution of the spectral state during the outburst. The HR shows a variability during the flare and the HR is varied between ~ 0.7 –6 for the time MJD 59210–59270. The hardness intensity diagram (HID) was studied using MAXI and HID did not show any significant change in spectral shape. Earlier the critical flux level was estimated to be $\sim 0.7 \times 10^{-9}$ erg cm $^{-2}$ s $^{-1}$. During the NICER observation of the 2021 outburst, the flux level was below the critical level. Above this flux level, the source state transition from sub-critical to super-critical accretion regime may occur and in this regime, the radiation pressure is high enough to halt the accretion flow at a certain height above the pulsar. During this transition, the pulse profile morphology, pulse fraction, and different spectral parameters also show some significant variation. The beaming pattern also seems to change from pencil beam to fan-beam or a mix of pencil and fan-beam (Becker et al. 2012).

Earlier a correlation between spin-up rate and X-ray flux was observed during outbursts for different transient systems, which were explained in terms of accretion. For example, 2S 1417–624 (Finger et al. 1996a), A 0535+26 (Finger et al. 1996b; Bildsten et al. 1997), EXO 2030+375 (Parmar et al. 1989; Reynolds et al. 1996), GRO J1744–28 (Bildsten et al. 1997), and SAX J2103.5+4545 (Baykal et al. 2002) showed correlation between spin-up rate and X-ray flux. Fig. 7 shows that the pulse frequency derivatives of the X-ray pulsar 2S 1417–624 are correlated with luminosity. Earlier for 2S 1417–624, Finger et al. (1996a) observed that $\dot{\nu}$ was highly correlated with the pulsed flux, both these parameters supposed to be driven by mass accretion rate.

Based on the accreting torque model and the observed spin-up rate, we have tried to find magnetic dipole moment and the surface magnetic field of 2S 1417–624. The spin-up rate and the luminosity are known to be correlated in transient X-ray pulsars as (Ghosh & Lamb 1979b; Sugizaki et al. 2017):

$$\dot{\nu}_{12} = 2.0n\zeta^{\frac{1}{2}}\mu_{30}^{\frac{2}{7}}R_6^{\frac{6}{7}}M_{1.4}^{-\frac{3}{7}}I_{45}^{-1}L_{37}^{\frac{6}{7}} \quad (2)$$

where $\dot{\nu}_{12}$, μ_{30} , R_6 , $M_{1.4}$, and I_{45} are the spin frequency derivative, magnetic dipole moment, radius, mass and the moment of inertia of the neutron star given in the units of 10^{-12} Hz s $^{-1}$,

10^{30} G cm^3 , 10^6 cm , $1.4 M_\odot$, and 10^{45} g cm^2 respectively. L is the X-ray luminosity in the unit of $10^{37} \text{ erg s}^{-1}$. According to the Ghosh & Lamb (1979a,b) model, under slow-rotator condition, $n \sim 1.39$ and $\zeta \sim 0.52$. Therefore, equation (1) reduces to (Sugizaki et al. 2017)

$$\dot{\nu}_{12} = k L_{37}^\alpha \quad (3)$$

where $k = 2.0 \mu_{30}^{\frac{2}{7}}$ and $\alpha = \frac{6}{7}$. For nominal values of $R_6 = M_{1.4} = I_{45} = 1$, measurements of the $\dot{\nu}$ versus L gives a rough estimation of the magnetic dipole moment of the pulsar. From the L vs $\dot{\nu}$ plot, we have estimated k and α as 7.65 ± 0.71 and 0.82 ± 0.11 respectively from the best fit result. The estimated value of α close to the theoretical value. Fig. 7 shows the correlation between the spin up rate and luminosity and the solid line represents the best fitted result. From the best fit result we may write the equation (2) as

$$\dot{\nu}_{12} = (7.65 \pm 0.71) L_{37}^{0.82 \pm 0.11} \quad (4)$$

Now the magnetic dipole moment can be written in the form

$$2.0 \mu_{30}^{\frac{2}{7}} = 7.65; \mu_{30} \simeq 109 \quad (5)$$

The surface magnetic field can be estimated using the magnetic moment (μ_{30}) and radius (R_6) of the pulsar as

$$\mu_{30} = \frac{1}{2} B_{12} R_6^3 \phi(x) \quad (6)$$

$\phi(x)$ is the correlation factor, for typical NS, $\phi(x) \sim 0.68$, the magnetic field can be written as

$$B_{12} = 2 \times \frac{\mu_{30}}{0.68} \quad (7)$$

for $\mu_{30} \simeq 109$, the magnetic field is estimated to be $\simeq 3 \times 10^{14} \text{ G}$.

The high value of magnetic dipole moment leads to a higher value of the magnetic field ($\sim 10^{14} \text{ G}$). This discrepancy mainly originates from the torque models, which do not allow closer distance (Malacaria et al. 2020). There are several sources like XTE J1858+034, GRO J1008–57, GS 0834–430, IGR J18179–1621, IGR J19294+1816, RX J0440.9+4431, MAXI J1409-619, and GRO J2058+42 for which considerable deviations from the GL model was observed even considering the Gaia measured distances (Malacaria et al. 2020). Earlier, Ji et al. (2020) also concluded that the estimated magnetic field and the distance to the source were relatively high. The distance of the source is taken as 10 kpc for the estimation of luminosity for this study. If the source distance is greater than the Gaia estimate ($\sim 20 \text{ kpc}$ (Ji et al. 2020)), then the magnetic field strength reduces to a typical value $\sim 10^{12} \text{ G}$.

Earlier, in 2013, Chandra observed the source during the quiescent phase. The pulsar spectrum was characterized with either a power-law or a blackbody model with a quite

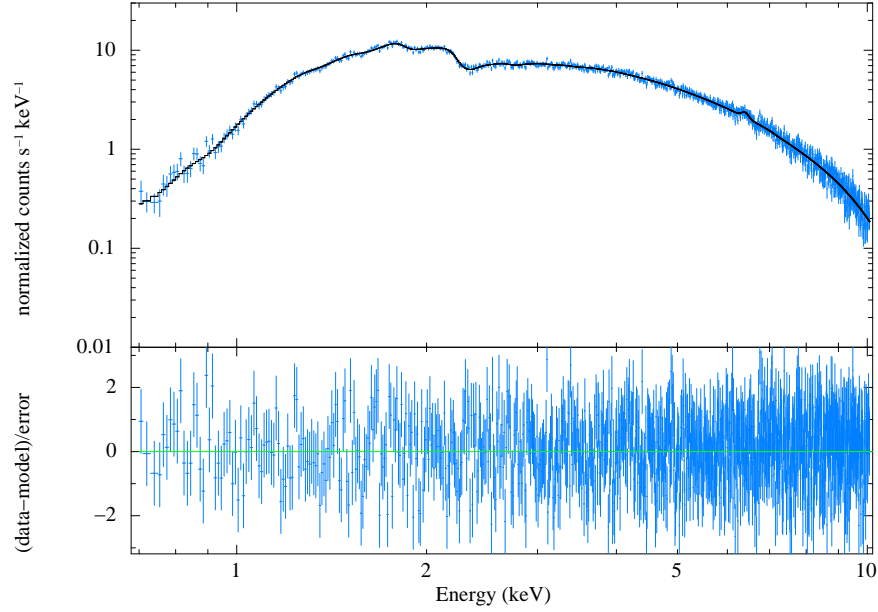


Fig. 8.— The energy spectrum of NICER/XTI (0.7–10 keV) with the best-fitted model $\text{phabs}*(\text{powerlaw}+\text{bbody}+\text{gaussian})$. Residual is shown in the bottom panel.

high temperature of ~ 1.5 keV (Tsygankov et al. 2017). The spectrum of the source during the 2021 outburst was well explained with a composite model of power-law and black-body components. During the 2018 giant outburst, the source spectrum was well explained with the cut-off PL continuum model and a BB component with the interstellar absorption (Gupta et al. 2019). The energy spectrum (NICER/XTI) of the source in the recent outburst in 2021 is also well described with a similar type of model as observed earlier. We have compared the spectral properties of the X-ray pulsar with the 2018 giant outburst at the same flux level. Earlier, photon index showed an anti-correlation with flux below $\sim 0.7 \times 10^{-9} \text{ erg cm}^{-2} \text{ s}^{-1}$. Such an anti-correlation was also observed in both 1999 (Inam et al. 2004) and 2009 outbursts (Gupta et al. 2018). During the recent outburst, the flux was below this limit and it was expected that the source was in a sub-critical accretion regime. We have compared the NICER spectrum close to the same flux level of the 2018 outburst and the result shows that the photon index decreases with the increase of X-ray flux and the spectrum get harder. We have tried to find the radius of the emitting region of the pulsar using the fitting parameters. The normalization constant of the blackbody model gives the size of the emission region for a known distance to the source. From the results of spectral fitting, the radius of the emitting region is ~ 0.98 km for a distance of ~ 10 kpc.

5. Conclusion

We have summarized the results of the timing and spectral analysis of the X-ray pulsar 2S 1417–624 during the outburst in 2021. The spin period was found to be ~ 17.3622 s using NICER/XTI observation and the spin-up rate varies between $\sim 0.8\text{--}1.8 \times 10^{-11}$ Hz s $^{-1}$ during the outburst. A positive correlation is observed between the spin-up rate and luminosity during the outburst. The torque-luminosity model gives a surface magnetic field of the pulsar $\sim 10^{14}$ G, the higher magnetic field may be arises due to the closer distance as given by Gaia. The pulse profile showed multiple peaks and dips which evolves with energy. A positive correlation of PF with energy was observed. The emission from the source evolved from softer to harder during the rising phase of the outburst and from harder to softer during the decay phase. The energy spectrum of the source was well described with a composite model consisting of power-law and a thermal blackbody component. The radius of the emitting region of the pulsar is estimated to be ~ 0.98 km.

Acknowledgements

This research has made use of the MAXI data provided by RIKEN, JAXA, and the MAXI team. We thank the duty scientists of the Neil Gehrels Swift Observatory for the extremely rapid and efficient scheduling of the observation. We acknowledge the use of public data from the Swift, NICER, and Fermi data archives.

Data Availability

The data underlying this article are publicly available in the High Energy Astrophysics Science Archive Research Center (HEASARC) at

<https://heasarc.gsfc.nasa.gov/db-perl/W3Browse/w3browse.pl>.

REFERENCES

- Apparao, K.M.V., Naranan, S., Kelley, R.L., Bradt, H.V., 1980. 2S 1417–624: a variable galactic X-ray source near CG 312–1, *A&A* 89, 249–250.
- Baykal, A., Stark, M.J., Swank, J.H., 2002. X-ray spectra and pulse frequency changes in SAX J2103.5+4545, *ApJ* 569(2), 903–910.

- Becker, P.A., Klochkov, D., Schönherr, G., et al., 2012. Spectral formation in accreting X-ray pulsars: bimodal variation of the cyclotron energy with luminosity, *A&A* 544, A123.
- Bildsten, L., Chakrabarty, D., Chiu, J., et al., 1997. Observations of Accreting Pulsars, *ApJS* 113(2), 367–408.
- Epili, P., Naik, S., Jaisawal, G.K., Gupta, S., 2017. Decade long RXTE monitoring observations of Be/X-ray binary pulsar EXO 2030+375, *MNRAS* 472(3), 3455–3466.
- Finger, M.H., Beklen, E., Narayana, B.P., et al., 2009. Long-term Monitoring of Accreting Pulsars with Fermi GBM, arXiv e-prints, arXiv:0912.3847.
- Finger, M.H., Wilson, R.B., Chakrabarty, D., 1996. Reappearance of the X-ray binary pulsar 2S 1417-624, *A&AS* 120, 209–212.
- Finger, M.H., Wilson, R.B., Harmon, B.A., 1996. Quasi-periodic Oscillations during a Giant Outburst of A0535+262, *ApJ* 459, 288.
- Gehrels, N., Chincarini, G., Giommi, P., et al., 2004. The Swift gamma-ray burst mission, *ApJ* 611(2), 1005–1020.
- Gendreau, K.C. Arzoumanianab, Z., Adkins, W.P., et al., 2016, *Proc. SPIE*, Vol. 9905, The Neutron Star Interior Composition Explorer (NICER): Design and Development, p. 99051H.
- Ghosh, P., Lamb, F.K., 1979a. Accretion by rotating magnetic neutron stars. II. Radial and vertical structure of the transition zone in disk accretion, *ApJ* 232, 259–276.
- Ghosh, P., Lamb, F.K., 1979b. Accretion by rotating magnetic neutron stars. III. Accretion torques and period changes in pulsating X-ray sources, *ApJ* 234, 296–316.
- Gupta, S., Naik, S., Jaisawal, G.K., Epili, P.R., 2018. Spectral and timing studies of 2S 1417-624 during a giant outburst, *MNRAS* 479(4), 5612–5619.
- Gupta, S., Naik, S., Jaisawal, G.K., 2019. NuSTAR view of Be/X-ray binary pulsar 2S 1417–624 during 2018 giant outburst, *MNRAS* 490(2), 2458–2466.
- Hazra, M., Pal, S., Mandal, M., et al., 2021. Swift/MAXI/Fermi detection of strong X-ray activity from 2S 1417–624, *The Astronomer’s Telegram*, 14349, 1.
- Hickox R. C., Narayan R., Kallman T. R., 2004. Origin of the Soft Excess in X-Ray Pulsars, *ApJ* 614, 881–896.

- İnam, S. Ç., Baykal, A., Matthew Scott, D., et al., 2004. X-ray flux related timing and spectral features of 2S 1417-62, MNRAS, 349(1), 173–180.
- Jaisawal, G.K., Naik, S., Epili, P., 2016. Suzaku view of the Be/X-ray binary pulsar GX 304–1 during Type I X-ray outbursts, MNRAS 457(3), 2749–2760.
- Ji, L., Doroshenko, V., Santangelo, A., et al., 2020. Timing analysis of 2S 1417-624 observed with NICER and Insight-HXMT, MNRAS 491(2), 1851–1856.
- Kabiraj, S., Paul, B., 2020. Broad-band X-ray characteristics of the transient pulsar GRO J2058+42, MNRAS 497(1), 1059–1065.
- Krimm, H.A., Holland, S.T., Corbet, R.H.D., et al., 2013. The Swift/BAT Hard X-ray Transient Monitor, ApJS 209(1), 14.
- Leahy, D.A., 1987. Searches for pulsed emission - Improved determination of period and amplitude from epoch folding for sinusoidal signals, A&A 180(1–2), 275–277
- Mandal, M., Pal, S., 2020. Study of Timing and Spectral Properties of the X-ray Pulsar A 0535+262 During the Giant Outburst in Nov-Dec 2020, arXiv, arXiv:2012.15839.
- Matsuoka, M., Kawasaki, K., Ueno, S., et al., 2009. The MAXI Mission on the ISS: Science and Instruments for Monitoring All-Sky X-Ray Images, PASJ 61, 999–1010.
- Meegan, C., Lichti, G., Bhat, P.N., et al., 2009. The Fermi gamma-ray burst monitor, ApJ 702(1), 791–804.
- Malacaria C., Jenke P., Roberts O. J., Wilson-Hodge C. A., Cleveland W. H., Mailyan B., GBM Accreting Pulsars Program Team, 2020. The Ups and Downs of Accreting X-ray Pulsars: Decade-long Observations with the Fermi Gamma-Ray Burst Monitor ApJ 896(1), 90.
- Naik, S., Maitra, C., Jaisawal, G.K., Paul, B., 2013. Timing and Spectral properties of Be/X-ray pulsar EXO 2030+375 during a Type I outburst, ApJ 764(2), 158.
- Parmar, A.N., White, N.E., Stella, L., 1989. The transient 42 second x-ray pulsar EXO 2030+375. II. The luminosity dependence of the pulse profile, ApJ 338, 373.
- Raichur, H., Paul, B., 2010. Apsidal motion in 4U 0115+63 and orbital parameters of 2S 1417–624 and V0332+53, MNRAS 406(4), 2663–2670.
- Reig, P., Nespoli, E., 2013. Patterns of variability in Be/X-ray pulsars during giant outbursts, A&A 551, A1.

- Reynolds, A.P., Parmar, A.N., Stollberg, M.T., Verbunt, F., Roche, P., Wilson, R.B., Finger, M.H., 1996. Accretion torques in the transient X-ray pulsar EXO 2030+375, *A&A* 312, 872.
- Sugizaki, M., Mihara, T., Nakajima, M., Makishima, K., 2017. Correlation between the luminosity and spin-period changes during outbursts of 12 Be binary pulsars observed by the MAXI/GSC and FERMI/GBM, *PASJ* 69(6), 100.
- Tsygankov, S.S., Wijnands, R., Lutovinov, A.A., Degenaar, N., Poutanen, J., 2017. The X-ray properties of Be/X-ray pulsars in quiescence, *MNRAS* 470(1), 126–141.